A Study on the Co-design of On-chip Varactor-based Gallium Nitride Microstrip Bandpass Filters

Andrés Fontana[*1], Dimitra Psychogiou[*#2]

[*]Tyndall National Institute, Ireland

[#]School of Engineering, University College Cork, Ireland

[1]afontana@ieee.org, [2]DPsychogiou@ucc.ie

***Abstract* — A study on the performance of continuously-tunable millimeter-wave varactor-based Monolithic Microwave Integrated Circuit (MMIC) bandpass filters (BPFs) is presented. An experimental characterization of Gallium Nitride on Silicon Carbide (GaN-on-SiC) varactors with different number of fingers and gate widths is carried out to determine their performance from 25 to 45 GHz. These results are used to improve the center frequency tuning range of a 2nd order Chebyshev BPF implemented with quarter-wavelength microstrip coupled resonators, while minimizing the in-band losses. A continuously tunable bandpass filter covering 5G New Radio Frequency Range 2 bands from 25-29.2 GHz, with 1 GHz bandwidth, and total insertion loss 3.4-6.7 dB is demonstrated.**

***Keywords* — bandpass filter, frequency tuning, monolithic microwave integrated circuit, tunable filter.**

I. INTRODUCTION

Highly-reconfigurable radiofrequency (RF) front-ends (RFFEs) are increasingly being considered for the next-generation of wireless communications to facilitate multi-standard operability or adaptivity to changing channel conditions. As the frequency rises to the millimeter-waves (mmWaves), RF-switched implementations are preferred to continuously tunable solutions due to the unloaded quality factor (Q_u) of varactors being low at high frequencies. However, they are limited to discrete pre-defined bands without sufficiently meeting the required levels of adaptivity [1]. Despite their technological limitations, varactors are the only path forward for continuously tunable RF circuits in advanced monolithic microwave integrated circuit (MMIC) technologies such as Gallium Nitride (GaN) that offer exceptional power density to frequencies as high as the mmWaves. Whereas GaN HEMT processes have been traditionally being used for the implementation of power amplifiers, their transistor capabilities have expanded, allowing for the realization of low-noise amplifiers [2] and phase shifters [3], among others.

Even though some GaN-based varactor RF characterizations have started to arise in the literature [4], [5], [6], very few mmWave continuously-tunable devices are reported. In [5], an automated network synthesis procedure to yield accurate on-chip varactor simulation models was introduced using GaN-on-SiC Schottky. The same devices were also used in [6], to evaluate their linear and non-linear behavior in two different GaN processes from C-to-K-band. Reported results exhibit varactors within 20-40 % tuning range and minimum Q_u of 5-8 at 26 GHz. In [7] a 60° to 165° tunable phase shifter with less than 8 dB loss was demonstrated at X-band, while a 7° to 30° phase shifter was reported in [8] at 29 GHz with an integrated amplifier for losses compensation. Even though bandpass filters (BPFs) are fundamental blocks in RF transceivers, to the best of the authors' knowledge no examples of continuously-tunable K-band examples have been reported. Tunable BPFs suffer from high insertion loss (IL) and limited frequency tuning range as a consequence of the capacitance tuning and Q_u of the varactor [9], [10]. In [11], GaAs single filter blocks based on active resonators were used to compensate for the IL at the expense of larger footprint and extra power consumption.

In this work, we introduce for the first time a study for the realization of continuously-tunable passive BPFs at Ka-band using bespoke varactors designed on a commercially-available GaN-on-SiC HEMT process. A set of transistor-based on-chip varactors are manufactured and characterized from 25 to 45 GHz, providing an insight into the trade-off between the capacitance tuning range and Q_u for wireless applications at these bands. Experimental results are leveraged to introduce an RF co-design technique for continuously-tunable BPFs with optimal performance in the 5G New Radio Frequency range 2 (FR2) bands n257/n258 having a frequency tuning range (Δf_0) = 25.07-29.21 GHz (16.5 %), IL= 3.4-6.7 dB, and fractional bandwidth (FBW) = 4%.

II. GaN VARACTORS CHARACTERIZATION

To assess the RF performance of GaN varactors at Ka-band, a set of 4- and 6-finger E-mode transistors featuring unit gate widths (*UGW*)=25 and 55 µm were used to design varactors on the NP12-01 process from WIN Semiconductors, which is a 0.12µm GaN-on-SiC HEMT technology manufactured on 100 mm wide SiC substrates. Fig. 1(a) shows a photograph of a manufactured 4-finger varactor with minimum *UGW* = 25 µm. An optimized E-mode transistor with outside back-via footprint was utilized to minimize the parasitic inductance and resistance of back-vias. The design also considered minimizing the required interconnection lines for biasing to reduce parasitics and losses. The equivalent circuit schematic of the varactor is provided in Fig. 1(b). To achieve the voltage-controlled total capacitance (C_T) behavior, the transistor is configured as a Metal-Oxide-Semiconductor (MOS) capacitor by grounding the drain and source terminals [10], [11]. The device is tuned by applying a DC voltage V_G=-6 to -1 V at the gate terminal through the bias network L_G=0.56 nH, C_G=0.56 pF, whilst the

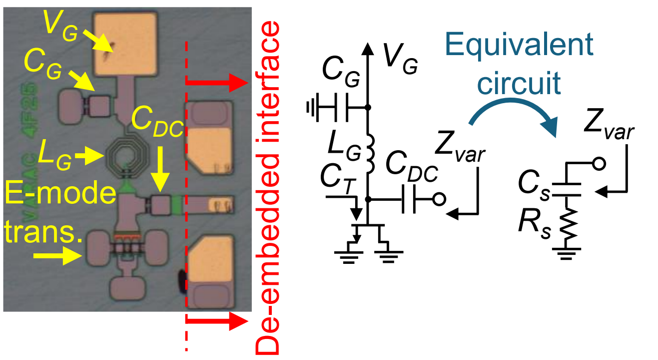

(a) (b)

Fig. 1. (a) Photograph of a GaN-on-SiC HEMT varactor using a 4x25 µm transistor. (b) Circuit schematic of the varactor and its equivalent model.

DC signal is decoupled from the RF port by means of a DC block with capacitance (C_{DC})=500 fF. The varactor network can be also represented by its simplified equivalent RC circuit, where $C_s = C_T // C_{DC}$ is the equivalent series capacitance of the varactor and R_s represents the losses of the overall device. Adjusting C_{DC} can help reduce the minimum C_s value in expense of capacitance tuning range.

A. GaN varactors RF characterization versus frequency

To extract C_s and R_s, on-wafer RF characterization measurements were carried out by means of a Keysight's N5247B PNA-X and an MPI's TS200 probe station testbench. The varactors were characterized from 25 to 45 GHz leveraging the valid frequency range of on-chip TRL calibration kits designed to de-embed the effect of testing pads (Fig. 1(a)). After applying a standard S-to-Y-parameter conversion, the equivalent RC circuit and its associated Q_u can be computed at every frequency using (1)-(3).

$$C_s(V_G, f) = I_m\{Y(1,1)\}/(2\pi f) \quad (1)$$
$$R_s(V_G, f) = R_e\{1/Y(1,1)\} \quad (2)$$
$$Q_s(V_G, f) = I_m\{Y(1,1)\}/ R_e\{Y(1,1)\} \quad (3)$$

Fig. 2 depicts the calculated C_s and Q_u as a function of frequency. As a worst-case scenario, all the tested samples were biased with V_{Gmin} = -1 V so that they exhibit the lowest self-resonant frequency (SRF) possible. Moreover, it is worth noting that as *UGW* and the number of fingers (*N*) is reduced, the SRF of the varactor shifts to higher frequencies. For instance, the measured devices exhibit $SRF|_{6x55\mu m}$= 31.4 GHz, $SRF|_{6x25\mu m}$= 38.2 GHz, and $SRF|_{4x55\mu m}$= 34.2 GHz, hindering their use for n259 and n260 bands (highlighted in light blue). However, the varactor with *N*=4 and UGW_{min} shows $SRF|_{4x25\mu m}$= 42.5 GHz. These devices also exhibit an undesired exponential capacitance variation (δC_s) that increases as the frequency reaches SRF. Their performance between 25-30 GHz is summarized in Table 1. Furthermore, the computed Q_u plots in Fig. 2(b) and detailed in Table 1 show higher Q_u as *N* and *UGW* are reduced. This is attributed to the lower metal contact resistance of the transistor terminals, the gate oxide, and the substrate losses [4].

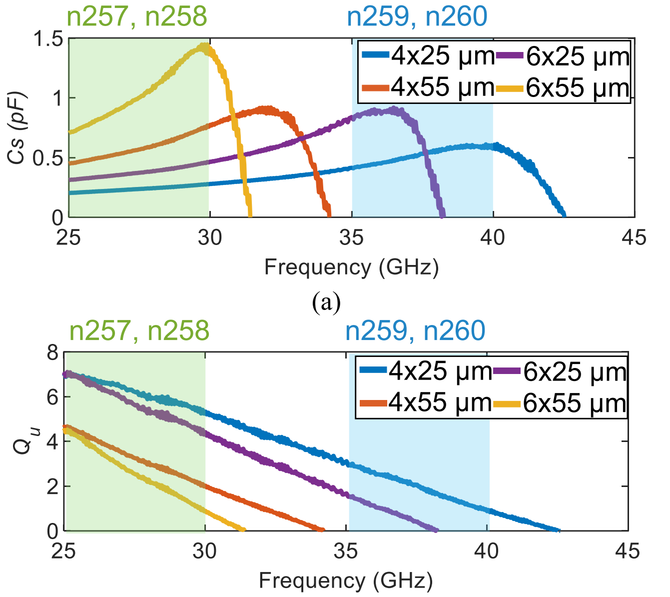

(b)

Fig. 2. Extracted C_s and Q_u as a function of frequency for different varactor types when biased with V_G = -1 V. (a) C_s. (b) Q_u.

B. Capacitance and Q_u tuning characterization

Once V_G is set, an ideal varactor should ensure a constant C_s ($\delta C_s \rightarrow 0$) across the frequency spectrum for the same bias voltage. As evidenced in Section II.A, the varactors with minimum *UGW* show the best performance in terms of Q_u and SRF, and a reduced exponential capacitance variation in frequency δC_s for a determined V_G. To better characterize the tuning capabilities of the 6x25 µm and 4x25 µm varactors, C_s and Q_u are plotted as a function of V_G in Fig. 3 at 26 GHz and 37 GHz. The C-V curves show the characteristic behavior of the MOS capacitors, with minimum capacitance C_{smin} for $V_G \leq$-3 V (inversion region), maximum capacitance C_{smax} for $V_G \geq$-1.25 V (accumulation region), and a tunable capacitance ΔC_S for -3 V ≤ $V_G \leq$-1.25 V (depletion region). Experimental results extracted from Fig. 3 are exhibited in Table 1. Even though in both varactor configurations Q_u is similar at 26 GHz, C_{smin} and ΔC_S are larger for the 6-finger varactor. At 37 GHz, C_{smin} and ΔC_S increase with frequency but Q_{umin} drops from 6.75 at 26 GHz to 0.65 at 37 GHz for the 6-finger varactor, and from 6.55 at 26 GHz to 2.2 at 37 GHz for the 4-finger varactor.

III. FR2 Tunable GaN BPF Implementation

Smaller varactors with minimum *N* and *UGW* are preferrable for extending Δf_0, enhancing Q_u, and reducing δC_S.

Table 1. Extracted C_s and Q_u for 4x25 µm, 4x55 µm, 6x25 µm, and 6x55 µm varactors as a function of frequency (*f* with V_G=-1 V), and bias voltage (V_G).

DUT	*f*=25 to 30 GHz			V_G=-6 to -1 V	
	$C_{s@25GHz}$ (fF)	δC_S (fF)	$Q_{u@25GHz}$/ $Q_{u@30GHz}$	$C_{smin}/C_{smax@26GHz}$ [ΔC_S] (fF)	$C_{smin}/C_{smax@37GHz}$ [ΔC_S] (fF)
4x25	203	76	6.9/5.3	103/216 [2.1:1]	191/499 [2.6:1]
4x55	450	321	4.7/2.0	224/493 [2.2:1]	N/A due to SRF
6x25	313	153	7.1/4.4	166/335 [2.0:1]	342/802 [2.3:1]
6x55	708	738	4.5/0.9	362/812 [2.2:1]	N/A due to SRF

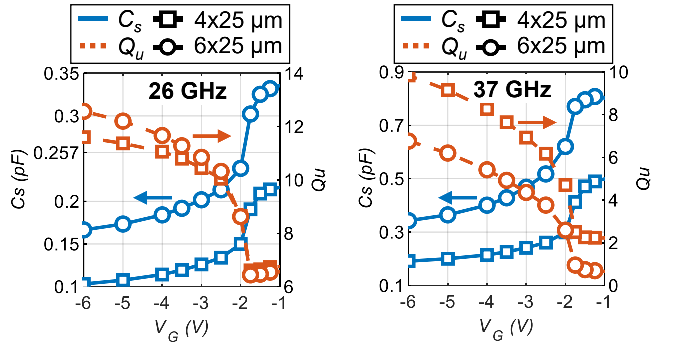

(a) (b)

Fig. 3. Extracted C_s and Q_u as a function of bias voltage V_G for the 4x25 µm and 6x25 µm GaN DUT varactors at (a) 26 GHz and (b) 37 GHz.

Nonetheless, smaller transistors result in lower C_{smin} and limited ΔC_S. To better estimate C_{smin}, ΔC_S, and Q_u, a study of their impact on Δf_0 and IL of a BPF is presented through a common second-order in-line two-resonator configuration using capacitively-loaded coupled-line resonators.

A. Frequency tuning study

The varactor circuit model in Section II is applied to a 2[nd] order Chebyshev BPF centered at 30 GHz with 3.3% FBW, and 0.045 dB in-band ripple. Its coupling routing diagram (CRD) and corresponding microstrip implementation using capacitively-loaded resonators and tapped port lines are illustrated in Fig. 4(a). Tunable resonators 2 and 3 can be represented as a shunt LC tanks, where L_0=0.324 nH and C_0=84 fF are the computed total inductance and capacitance of a quarter-wavelength microstrip resonator at f_0 = 30 GHz with length (L)=937 µm. The equivalent model of the varactor can be also represented as a parallel RC network (C_p, R_p) by converting Z_{var} to admittance to calculate the total resonant capacitance (C_0+C_p). As depicted in Fig. 4(b), the synthesized response of a BPF loaded with an ideal lossless varactor with C_{smin}=0 (Case 1) can be reconfigured from 30 to 25 GHz by tuning ΔC_s between 0-38 fF. However, if C_{smin}> 0 fF, the f_0 of the loaded resonator shifts towards lower frequencies. For example, when implementing a simulated 2x60 µm varactor with C_{smin}=64 fF (Case 2), the microstrip line must be shortened from 937 µm to 628 µm to adjust f_0 back to 30 GHz as shown in Table 2. As illustrated in Fig. 4(b), the modification of L_0 and C_0 reduces the frequency tuning Δf_0 for the same ΔC_s=0-38 fF. This effect is exacerbated as C_{smin} increases as in the case of 4x25 µm (Case 3) and 6x25 µm (Case 4) varactors, requiring larger ΔC_s to achieve the same tuning range (see Table 2). As

Table 2. Calculated values of a varactor-loaded microstrip resonator.

Case	C_{smin} (fF)	L (µm)	L_0 (nH)	C_0 (fF)	ΔC_S (fF)	Δf_0 (GHz)
1: Ideal	0	937	0.324	84	38	25-30[#]
2:2x60	64	628	0.235	56	38/ 50[†]	25.92-30[#]/ 25-30
3:4x25	110	468	0.185	42	38/ 65[†]	26.83-30[#]/ 25-30
4:6x25	184	312	0.132	29	38/ 95[†]	27.58-30[#]/ 25-30

[#]Δf_0 calculated for ΔC_s=38 fF. [†]ΔC_s needed for Δf_0=25-30 GHz.

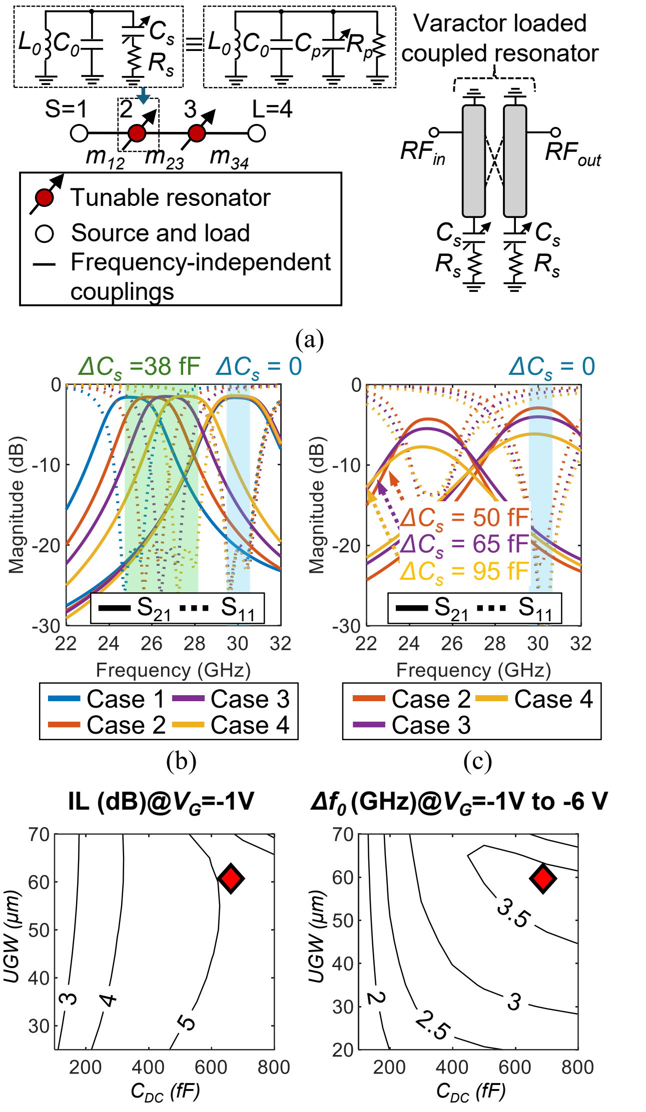

(d)

Fig. 4. (a) Tunable BPF CRD and its varactor-loaded coupled resonator implementation with tapped port lines. (b) Synthesized S-parameter response of the BPF in (a) with normalized coupling factors m_{11}=m_{22}= 0, m_{12}=m_{34}=1.22, and m_{23}=1.65 for lossless varactors (R_s=0 Ω) with ΔC_s =0-38 fF, C_{smin} = 0 (Case 1), C_{smin} = 64 fF (Case 2), C_{smin} = 110 fF (Case 3), C_{smin} = 184 fF (Case 4). (c) Synthesized S-parameter response of the cases shown in (b) for lossy varactors (R_s=2 Ω) with ΔC_s =0-50 fF (Case 2), ΔC_s =0-65 fF (Case 3), and ΔC_s =0-95 fF (Case 4). (d) Δf_0 and IL contour plots as a function of C_{DC} and UGW (N=2) of the coupled resonator BPF. The red marker highlights the chosen design point.

shown in Fig. 3, ΔC_s can be extended by increasing N, leading to an increase in C_{smin}, a further reduction of L, and once again, the need for larger ΔC_s. A similar effect can be observed when increasing UGW. Table 2 summarizes the extracted values of ΔC_s needed to meet the original Δf_0=25-30 GHz for Case 1-4.

B. Passband insertion loss

The impact of varactors with large C_{smin} and ΔC_s on the performance of the BPF can be observed in Fig. 4(c) where the effect of a lossy varactor (R_s=2 Ω) on Cases 2, 3 and 4 is studied. A degradation of IL can be noted as C_{smin} increases, as a result of the larger total capacitance of the resonator and the lower loaded quality factor Q_L=2πf_0R_p(C_0+C_p)=78, 33, and 17 for

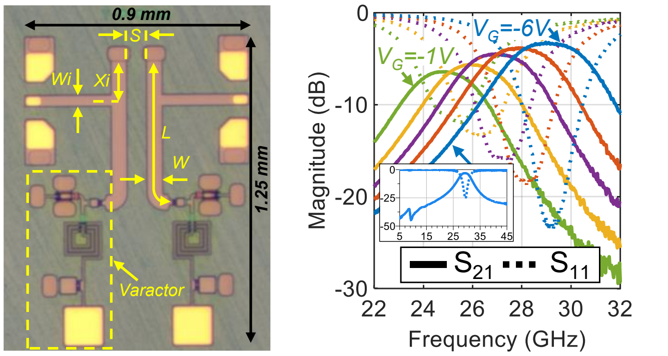

(a) (b)

Fig. 5. (a) Photograph of a GaN-on-SiC HEMT tunable mmWave BPF for a coupled resonator with dimensions W_i=47 µm, X_i=156 µm, W=64 µm, L=628 um, S=78 µm and 2x60 µm varactors with C_{DC}=0.65 pF, L_G=0.56 nH, and C_G=1.2 pF. (b) Measured S-parameters for V_G from -6 to -1 V (C_s=92-136 fF).

Cases 2, 3, and 4, respectively. In comparison to the lossless BPFs shown in Fig. 4(b) where $IL_{@25\,GHz}$= $IL_{@30\,GHz}$≈1.5 dB, the simulated devices in Fig. 4(c) exhibit: Case 2: $IL_{@25\,GHz}$= 4.3 dB and $IL_{@30\,GHz}$=2.9 dB; Case 3: $IL_{@25\,GHz}$= 5.5 dB and $IL_{@30\,GHz}$=4 dB; and Case 4: $IL_{@25\,GHz}$= 7.8 dB and $IL_{@30\,GHz}$=6.2 dB. Therefore, the varactor parameters *UGW*, *N*, and C_{DC} should be designed to have the minimum C_{smin} possible and sufficient ΔC_s to meet the necessary Δf_0 and degrading IL as little as possible. Fig. 4(d) depicts the Δf_0 and IL_{max} contour plots of the simulated coupled resonator BPF in function of C_{DC} and *UGW* for a 2-finger varactor, where Δf_0= 4 GHz and IL_{max}= 5.3 dB can be obtained with C_{DC}= 650 fF, and *UGW* = 60 µm.

IV. Experimental Validation

Fig. 5(a) depicts a photograph of a 1.25 mm x 0.9 mm co-designed tunable BPF manufactured using a commercially-available GaN-on-SiC HEMT process from WIN Semiconductors. The device was characterized using the same setup described in Section II. Measurement results (Fig. 5(b)) demonstrate a Δf_0=25.07-29.21 GHz (Δf_0=16.5%) and IL=3.4-6.7 dB, corresponding to an extracted 2x60 µm varactor with C_s=92-136 fF and R_s=2.22-3.65 Ω. In-band IL remains better than 5.5 dB from 26 to 29.21 GHz with return loss better than 10 dB. An FBW = 3.72–6.6 % and noise figure (NF)=4.2-6.8 dB is also obtained for the whole frequency tuning range.

Table 3 provides a comparison with state-of-the-art tunable bandpass filters developed on III-V technologies. The proposed BPF implementation concept is the only one implemented using GaN technologies. It demonstrates better IL_{min} than other similar GaAs devices while they operate at significantly lower frequencies. Furthermore, the IL_{max} remains similar than [10], operating at 2.53 GHz. Regarding Δf_0, other examples exhibit a larger frequency range than 16.5%, but it should be considered that the prototype in Fig. 5 was design to cover n257 and n258.

V. Conclusion

This work extends the body of knowledge on continuously-tunable GaN mmWave devices by introducing for the first time a study on the performance of transistor-varactor-based MMIC BPF at FR2. On-chip varactors with different numbers of fingers and gate widths were experimentally characterized on a GaN-on-SiC platform from 25 to 45 GHz. An RF co-designed methodology to maximize tuning range while reducing IL was demonstrated through a 2nd order Chebyshev BPF. Measured results show tunable BPF operation from 25.07-29.21 GHz, with 1 GHz bandwidth, and total insertion loss 3.4-6.7 dB.

Table 3. Comparison to state-of-the-art continuously-tunable bandpass filters.

Tech.	Tuning method	f_0 (GHz)	Δf_0 (%)	IL (dB)	NF (dB)	Size (λ_g x λ_g)	Ref.
GaAs pHEMT	Switch	10	30.6	4.1	N.A.	0.08x0.11	[12]
	Varactor	2.53	24.9	3-6.7	N.A.	3.75x1.84†	[10]
	Varactor	12	50	4.2	5	0.43x0.16	[9]
GaN HEMT	**Varactor**	**29.21**	**16.5**	**3.4-6.7**	**4.2-6.8**	**0.33x0.24**	**T.W.**

λ_g: guided wavelength, †in mm^2. T.W.: This work. N.A: Not available.

Acknowledgment

The authors would like to acknowledge WIN Semiconductors for providing the manufactured samples. This work was supported by Research Ireland (RI), Grant numbers 20/RP/8334 and 13/RC/2077_P2.

References

[1] R. Malmqvist, M. Khedri and R. Jonsson, "High-Linearity and Low-Noise Tunable C/X-Band GaN Filters for Robust Highly Integrated Front-Ends," *2024 19th European Microwave Integrated Circuits Conference (EuMIC)*, Paris, France, 2024, pp. 323-326.

[2] W. Ye, J. Zhou, H. Gao, H. Guo, Y. Gu and X. Zou, "1.48-dB-Noise Figure E-Mode Recessed-Gate GaN MOSHEMT by Argon-Based Neutral Beam Etching for LNA Applications," in *IEEE Transactions on Electron Devices*, vol. 72, no. 3, pp. 1035-1040, Mar. 2025.

[3] H. Zhao, X. Yan, H. Chu, X. Zhu and Y. Guo, "A 360° Tunable Phase Shifter With Low Phase Error Based on Bandpass Networks in 0.25-µm GaN Technology," in *IEEE Transactions on Very Large Scale Integration (VLSI) Systems,* Early Access, 2024.

[4] A. Hamdoun, L. Roy, M. Himdi and O. Lafond, "Characterization of GaN-based HEMTs as varactor diode devices," *2015 European Microwave Conference (EuMC)*, Paris, France, 2015, pp. 1268-1271.

[5] S. Cangini *et al*., "Empirical Equivalent-Circuit Modeling of mm-Wave GaN MMIC Varactors by Network Synthesis," in *IEEE Transactions on Microwave Theory and Techniques*, Early Access, 2025.

[6] S. Cangini *et al*., "Evaluation of Integrated GaN Diodes as Varactors for Tunable MMIC PAs from C- to K-Band," *2024 19th European Microwave Integrated Circuits Conference (EuMIC)*, Paris, France, 2024, pp. 14-17.

[7] M. Robinson, P. Danielson and Z. Popović, "Continuous Broadband GaAs and GaN MMIC Phase Shifters," in *IEEE Microwave and Wireless Components Letters*, vol. 32, no. 1, pp. 56-59, Jan. 2022.

[8] P. Neininger *et al*., "A Phase Shifter with Integrated PA MMIC for Ka-Band Frequencies," *2020 German Microwave Conference (GeMiC)*, Cottbus, Germany, 2020, pp. 13-16.

[9] F. Bergeras *et al*., "Novel MMIC architectures for tunable microwave wideband active filters," *2010 IEEE MTT-S International Microwave Symposium*, Anaheim, CA, USA, 2010, pp. 1356-1359.

[10] J. Li *et al*., "Reconfigurable GaAs Bandpass Filters Using Cascading of Lowpass and Highpass Filters," *2022 Asia-Pacific Microwave Conference (APMC)*, Yokohama, Japan, 2022, pp. 773-775.

[11] D. Simpson and D. Psychogiou, "GaAs MMIC Nonreciprocal Single-Band, Multi-Band, and Tunable Bandpass Filters," in *IEEE Transactions on Microwave Theory and Techniques*, vol. 71, no. 6, pp. 2439-2449, Jun. 2023.

[12] H. -R. Zhu, X. -Y. Ning, Z. -X. Huang and X. -L. Wu, "An Ultra-Compact On-Chip Reconfigurable Bandpass Filter With Semi-Lumped Topology by Using GaAs pHEMT Technology," in *IEEE Access*, vol. 8, pp. 31606-31613, 2020.